




Differentiation between renal epithelioid angiomyolipoma and clear cell renal cell carcinoma using clear cell likelihood score

Yu-Wei Hao¹ · Yun Zhang^{1,2} · Hui-Ping Guo¹ · Wei Xu¹ · Xu Bai¹ · Jian Zhao¹ · Xiao-Hui Ding³ · Sheng Gao⁴ · Meng-Qiu Cui¹ · Bai-Chuan Liu¹ · Hui-Yi Ye¹ · Hai-Yi Wang¹ 

Received: 18 May 2023 / Revised: 21 August 2023 / Accepted: 23 August 2023 / Published online: 25 September 2023
© The Author(s), under exclusive licence to Springer Science+Business Media, LLC, part of Springer Nature 2023

Abstract

Purpose Clear cell likelihood score (ccLS) may be a reliable diagnostic method for distinguishing renal epithelioid angiomyolipoma (EAML) and clear cell renal cell carcinoma (ccRCC). In this study, we aim to explore the value of ccLS in differentiating EAML from ccRCC.

Methods We performed a retrospective analysis in which 27 EAML patients and 60 ccRCC patients underwent preoperative magnetic resonance imaging (MRI) at our institution. Two radiologists trained in the ccLS algorithm scored independently and the consistency of their interpretation was evaluated. The difference of the ccLS score was compared between EAML and ccRCC in the whole study cohort and two subgroups [small renal masses (SRM; ≤ 4 cm) and large renal masses (LRM; > 4 cm)].

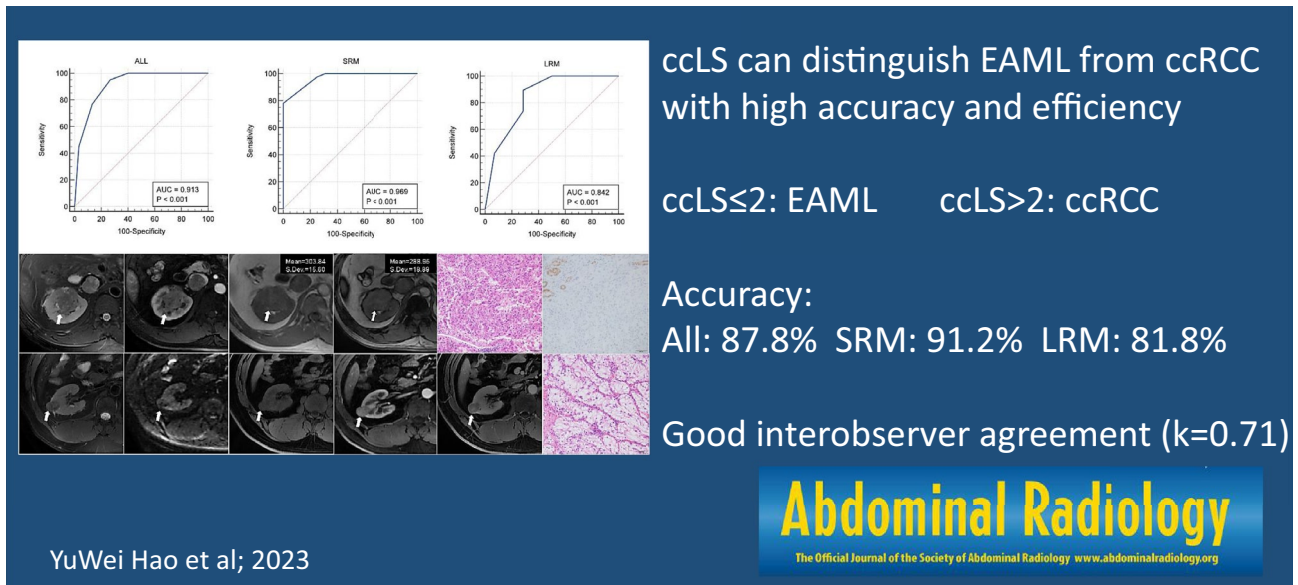
Results In total, 87 patients (59 men, 28 women; mean age, 55 ± 11 years) with 90 renal masses (EAML: ccRCC = 1: 2) were identified. The interobserver agreement of two radiologists for the ccLS system to differentiate EAML from ccRCC was good ($k = 0.71$). The ccLS score in the EAML group and the ccRCC group ranged from 1 to 5 (73.3% in scores 1–2) and 2 to 5 (76.7% in scores 4–5), respectively, with statistically significant differences ($P < 0.001$). With the threshold value of 2, ccLS can distinguish EAML from ccRCC with the accuracy, sensitivity, specificity, positive predictive value (PPV), and negative predictive value (NPV) of 87.8%, 95.0%, 73.3%, 87.7%, and 88.0%, respectively. The AUC (area under the curve) was 0.913. And the distribution of the ccLS score between the two diseases was not affected by tumor size ($P = 0.780$).

Conclusion The ccLS can distinguish EAML from ccRCC with high accuracy and efficiency.

Yu-Wei Hao and Yun Zhang have contributed equally as first authors.

Extended author information available on the last page of the article

Graphical Abstract



Keywords Angiomyolipoma · Carcinoma · Renal cell · Magnetic resonance imaging · Kidney neoplasms

Abbreviations

ccLS	Clear cell likelihood score
ccRCC	Clear cell renal cell carcinoma
EAML	Renal epithelioid angiomyolipoma
SRM	Small renal masses
LRM	Large renal masses
WHO	World health organization
MRI	Magnetic resonance imaging
PACS	Picture archiving and communication system
PPV	Positive predictive value
NPV	Negative predictive value
ROC	Receiver operating characteristic curve
AUC	Area under the curve
CI	Confidence interval
DWI	Diffusion-weighted imaging
ADER	Arterial-delayed enhancement ratio
SEI	Segmental enhancement inversion

Introduction

Renal epithelioid angiomyolipoma (EAML) is a rare variant of angiomyolipoma (AML), which accounts for 4.6–4.8% of all AML [1, 2]. Since 2004, EAML has been classified separately histologically and is defined as a renal mesenchymal neoplasia with malignant potential by the WHO [3, 4]. In general, EAML contains little or no adipose tissue [5–8]. The pathological criteria for diagnosing EAML is the presence of at least

80% epithelioid cells in the tumor [1, 2, 9]. Pathologically, the tumor showed obvious pleomorphism and nuclear atypia, accompanied by hemorrhage, necrosis, and cystic degeneration [10, 11]. Originating from the renal proximal tubule, clear cell renal cell carcinoma (ccRCC), is the most common histological subtype of renal cell carcinoma (RCC) which accounts for about 75–80% of RCC [9]. In addition to its rich neovascularization, ccRCC also exhibits hemorrhagic, cystic, and necrotic features [12–15]. Therefore, EAML is often misdiagnosed as ccRCC. Patients with ccRCC are usually surgical candidates. Patients with EAML smaller than 4 cm can be active surveillance through regular follow-up, on the other hand, patients with EAML larger than 4 cm go to surgery as their risk of bleeding is high. Treatment strategy and prognosis are quite different between the two entities. It is particularly important to make a correct diagnosis before surgery.

Several studies have examined the identification methods of EAML and ccRCC, however, the results may be less than ideal. Renal mass biopsy is a useful method, but it is an invasive procedure, also exposed to false-negative results [16]. The rate of missed diagnosis is as high as 20% [17]. Magnetic resonance imaging (MRI) is useful for determining the subtypes of RCC [18–21]. MR imaging features of EAML are not specific and the literature on EAML is limited to descriptive studies [22–25]. It is challenging to distinguish EAML and ccRCC through conventional imaging characteristics analysis. Clear Cell Likelihood Score (ccLS; 1-very unlikely, 2-unlikely, 3-equivocal, 4-likely, and 5-very likely) based on a Likert scale

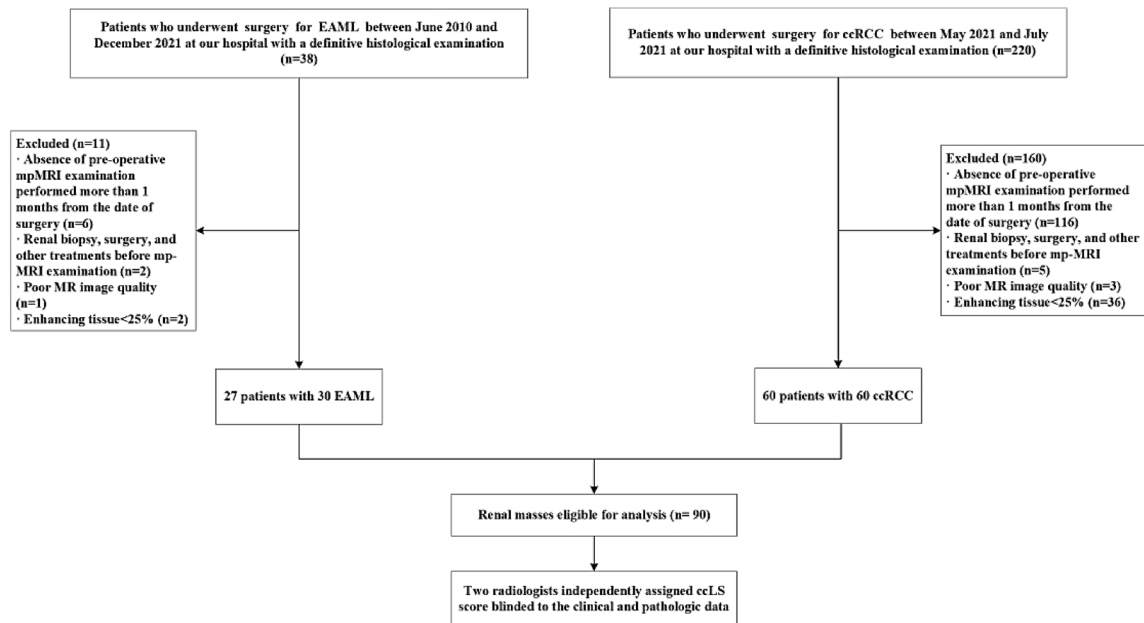


Fig. 1 Flowchart of the study cohort. *ccRCC* clear cell renal cell carcinoma, *EAML* renal epithelioid angiomyolipoma, *ccLS* clear cell likelihood score

is a novel method for the diagnosis and differential diagnosis of solid renal tumors [26–28]. It utilizes standardized diagnostic algorithms to assign a ccLS score to each lesion based on T2WI signal intensity, corticomedullary enhancement, and microscopic fat [29]. The scoring system minimizes the influence of radiologists' experience and could serve as a reference tool for junior radiologists in their daily diagnosis work. Using the ccLS algorithm, Canvasser et al. carried out a retrospective analysis of 67 small renal masses (SRM) and found that the accuracy of the scoring system in diagnosing ccRCC and non-ccRCC was 84% and 86%, respectively [28]. In a retrospective analysis of 102 renal masses, Dunn et al. found that the accuracy of the scoring system in diagnosing ccRCC in the cT1a and cT1b stages was 83% and 92%, respectively [30]. Nevertheless, it is not clear whether ccLS is a reliable diagnostic method for distinguishing EAML and ccRCC.

In this study, we aimed to investigate the ccLS in the differential diagnosis between EAML and ccRCC, hoping to provide an alternative approach for the accurate identification of these two entities

Methods

Ethical approval

This retrospective cohort study was approved by the Ethics Committee and Institutional Review Board of our institution (S2021-070-01). Written informed consent was not required

for this study because only fully anonymized MR images have been used.

Study population

Between June 2010 and December 2021, patients who underwent surgery for EAML at our hospital with a definitive histological result ($n = 38$) were collected, as well as patients who underwent surgery for ccRCC between May 2021 and July 2021 with a definitive histological result ($n = 220$) (Fig. 1). All the lesions were larger than 1 cm. Exclusion criteria: (a) absence of pre-operative mp-MRI examination performed more than 1 month from the date of surgery ($n = 6$ and $n = 116$, respectively); (b) renal biopsy, surgery, and other treatments before MRI examination ($n = 2$ and $n = 5$, respectively); (c) poor MR image quality (motion artifacts; low image resolution, etc.) ($n = 1$ and $n = 5$, respectively); (d) $<25\%$ enhancement ($n = 2$ and $n = 36$, respectively).

MRI acquisition

MR imaging was performed on 1.5 T (GE Signa HDxt, Philips Multiva, and uMR570) and 3.0 T (GE Discovery MR750 and uMR770) systems using a surface phased-array coil. Renal MRI protocols included axial fat-saturated T₂-weighted single-shot fast spin-echo imaging, the diffusion-weighted sequence with low ($50 \text{ mm}^2/\text{sec}$) and high

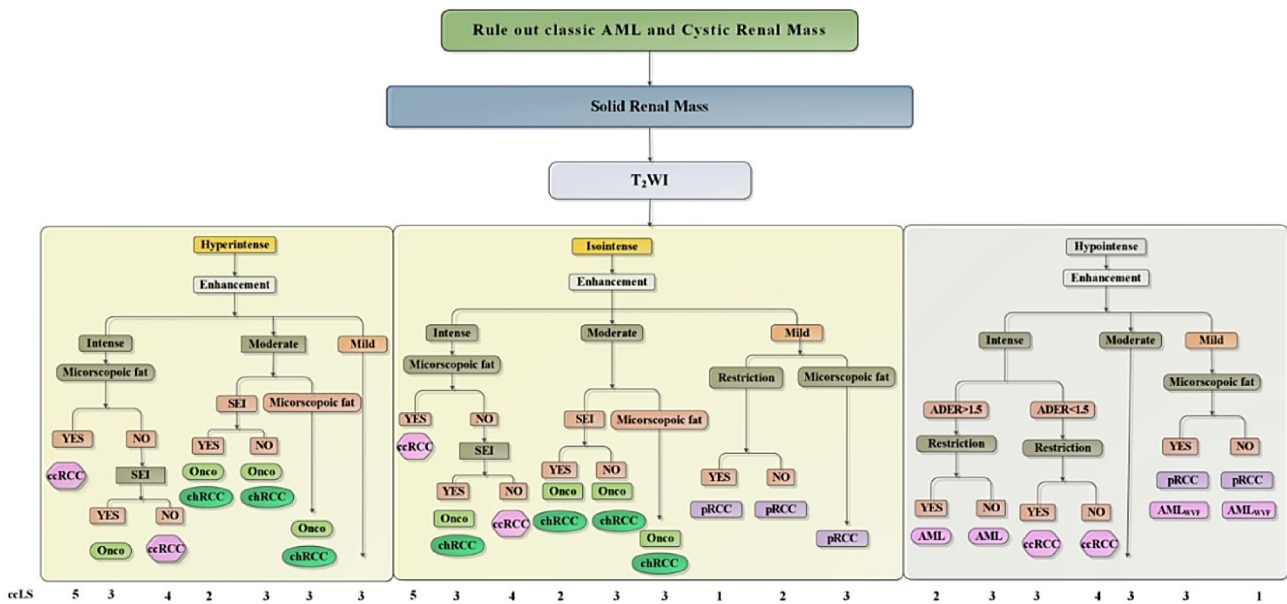


Fig. 2 Clear cell likelihood score (ccLS) diagnostic algorithm and image interpretation. Presence of enhancement in at least 25% of the mass and absence of macroscopic fat represent eligibility criteria for use of the ccLS algorithm. Signal intensity at T2-weighted single-shot fast spin-echo imaging (T2) relative to renal cortex, enhancement during the corticomedullary phase relative to renal cortex, and presence of microscopic fat are major criteria evaluated in every mass. Restriction in diffusion-weighted imaging (DWI), segmental enhancement inversion (SEI), and arterial-to-delayed enhance-

ment ratio (ADER) are ancillary findings, which are assessed when indicated in the algorithm. *AML* angiomyolipoma, *ccRCC* clear cell renal cell carcinoma, *chRCC* chromophobe renal cell carcinoma, *Onco* oncocytoma, *pRCC* papillary renal cell carcinoma, *Start* arterial phase signal intensity (SI); *Slpre* pre-contrast SI; *Slidel* delayed phase SI. (From Pedrosa I, Cadeddu JA. How We Do It: Managing the Indeterminate Renal Mass with the MRI Clear Cell Likelihood Score. *Radiology*. 2022 Feb;302(2):256-269; with permission.)

(800 mm²/sec) *b* value, axial chemical shift T₁-weighted imaging, and dynamic contrast-enhanced T₁-weighted imaging. MRI equipment and protocols used are shown in Tables E1–E4.

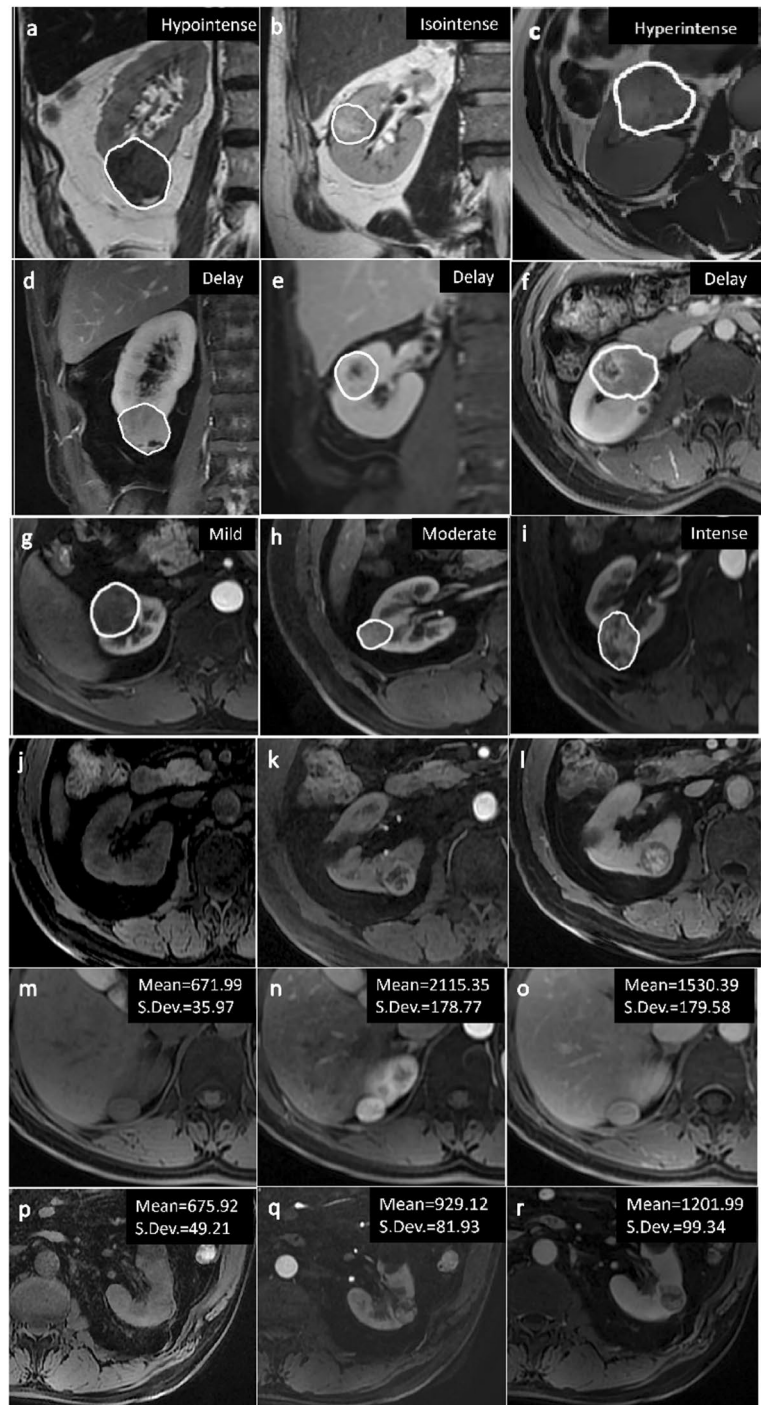
Imaging analysis and ccLS evaluation

Clear Cell Likelihood Score was defined as 1-very unlikely, 2-unlikely, 3-equivocal, 4-likely, and 5-very likely. Before the formal evaluation, two radiologists (Y.W.H and Y.Z., with 3 years and 12 years of experience in genitourinary diagnosis, respectively) reviewed the ccLS scoring criteria in detail and performed the simulation evaluation to ensure that could properly use utilize this diagnostic tool. After the fellowship training and example case presentation, two radiologists who were blinded to the clinical and pathologic data, reviewed each tumor on the institutional picture archiving and communication system (PACS, DJ HealthUnion Systems Corporation) independently (Table E5).

For each radiologist, the following imaging features were observed and all lesions were scored based on the criteria of ccLS algorithm as follows [29, 31–33]. The interobserver agreement of ccLS between the two readers was evaluated.

Major criteria: (a) signal intensity on T2-weighted images (recorded as hypointense, isointense or hyperintense to the renal cortex). Only the solid component of the lesion was evaluated, avoiding cystic degeneration, necrotic areas, and tumor margins. Hyperintense on T2WI is defined as the predominant tumor signal intensity (> 50% solid component) is higher than the renal cortex; isointense on T2WI is defined as the predominant tumor signal intensity (> 50% solid component) is similar to the renal cortex; hypointense on T2WI is defined as the predominant tumor signal intensity (> 50% solid component) is lower than the renal cortex; (b) corticomedullary enhancement (calculated as intense (> 75%), moderate (45–75%), or mild (< 40%) enhancement to the renal cortex on the corticomedullary phase). Note that only the most intense contrast enhancement of the lesion on the basis of visual should be evaluated. The calculation formula is: $[(T_{CM} - T_{pre}) / T_{pre}] / [(C_{CM} - C_{pre}) / C_{pre}] \times 100\%$. T_{CM} and C_{CM} : the tumor and cortex corticomedullary SI; T_{pre} and C_{pre} : the tumor and cortex SI before contrast enhancement; (c) microscopic fat (recorded as present or absent), refers to the fact that an unequivocal drop of signal intensity comparing T1-weighted gradient-echo out-phase to in-phase images. When the subjective evaluation is uncertain, it can be quantified by delineating the ROI. The standard is

Fig. 3 The imaging parameters of clear cell likelihood score (ccLS) (a–z). White outlines delineate the boundaries of renal masses. Signal intensity on T2-weighted images (hypointense, isointense or hyperintense) are shown in these images. Firstly, the enhancing portions of the tumor should be determined on the delayed phase (d–f), then signal intensity of the majority of the tumor compare to the renal cortex on T2-weighted images should be evaluated (a–c). Corticomedullary enhancement (mild, moderate, or intense) are shown in these images (g–i). The images should be interpreted as presence of segmental enhancement inversion (j–l). The images show that arterial-to-delayed enhancement ratio was 1.68, which was higher than 1.5 (m–o). The images show that arterial-to-delayed enhancement ratio was 0.48, which was less than 1.5 (p–r). The images should be interpreted as presence of microscopic fat. Quantitative assessment was shown ($SI_{\text{tumor.IP}} - SI_{\text{tumor.OP}} > (SD_{\text{IP}} + SD_{\text{OP}})$) (s, t). The images should be interpreted as absence of microscopic fat. Quantitative assessment was shown ($SI_{\text{tumor.IP}} - SI_{\text{tumor.OP}} < (SD_{\text{IP}} + SD_{\text{OP}})$) (u, v). The images should be interpreted as presence of marked restriction (w, x). The images should be interpreted as no marked restriction (y, z). $SI_{\text{tumor.IP}}$ and $SI_{\text{tumor.OP}}$ is the signal intensity of tumor at in-phase imaging and out-phase imaging, and $SD_{\text{tumor.IP}}$ and $SD_{\text{tumor.OP}}$ is the standard deviation of the tumor at in-phase imaging and out-phase imaging



defined as $(SI_{\text{tumor.IP}} - SI_{\text{tumor.OP}}) > (SD_{\text{IP}} + SD_{\text{OP}})$, where $SI_{\text{tumor.IP}}$ and $SI_{\text{tumor.OP}}$ is the signal intensity of the tumor at in-phase imaging and out-phase imaging, and $SD_{\text{tumor.IP}}$ and $SD_{\text{tumor.OP}}$ is the standard deviation of the tumor at in-phase imaging and out-phase imaging.

Ancillary features: (a) marked restriction on diffusion-weighted images (DWI, recorded as present or absent), refers to the fact that the lesions show the high signal on high b DWI and low signal on ADC; (b) segmental enhancement

inversion (SEI, recorded as present or absent), refers to the fact that in the corticomedullary phase, the enhancement degree of the two regions of the tumor is different, whereas, in the delayed phase, the enhancement degrees are reversed; (c) arterial-to-delayed enhancement ratio (ADER, $SI_{\text{art}} - SI_{\text{pre}} / SI_{\text{del}} - SI_{\text{pre}}$, where SI_{art} , SI_{pre} and SI_{del} is the signal intensity of the tumor in the corticomedullary phase, pre-contrast phase and delayed phase, respectively), similar to “washout”, refers to the lesions showing avid enhancement

Fig. 3 (continued)

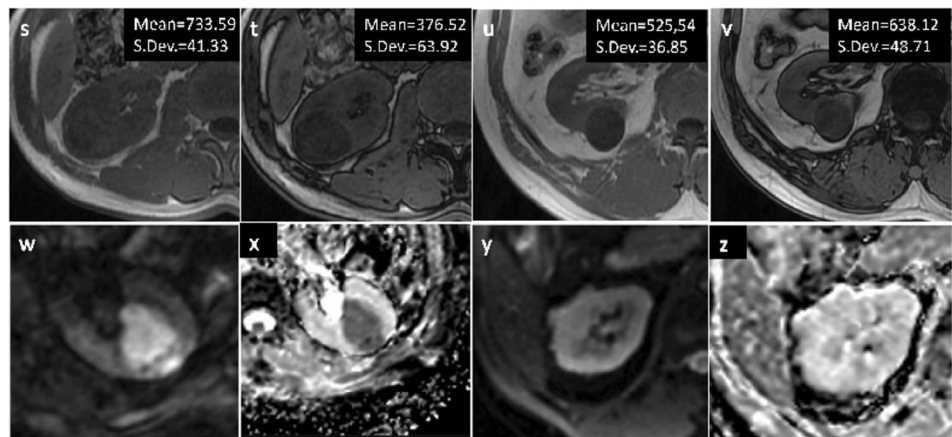


Table 1 Clinical data of patients with EAML and ccRCC

	EAML	ccRCC	P value
No. of patients (%)	27 (31%)	60 (69%)	
No. of lesions (%)	30 (33%)	60 (67%)	
Mean tumor size (cm) ± SD	5.4±4.5 (1.1–14)	3.6±2.3 (1.2–22)	< 0.001*
Gender			< 0.001*
Male	11 (41%)	48 (80%)	
Female	16 (59%)	12 (20%)	
Mean age (years) ± SD	40±5	57±10	< 0.001*
Side			0.655
Left	14 (47%)	31 (52%)	
Right	16 (53%)	29 (48%)	
Mean BMI ± SD	24.3±3.2	26.3±5.7	0.08
Symptom			0.129
Yes	8 (30%)	8 (13%)	
No	19 (70%)	52 (87%)	
Smoking history	4 (15%)	28 (47%)	0.004*
Drinking history	7 (26%)	38 (63%)	< 0.001*
Hypertension history	4 (15%)	31 (52%)	< 0.001*
Diabetes history	0 (0%)	12 (20%)	0.03*
Surgery			0.14
RN	13 (48%)	19 (32%)	
PN	14 (52%)	41 (68%)	

Quantitative data are presented in the form of mean, median (inter-quartile range, IQR)
EAML renal epithelioid angiomyolipoma, *ccRCC* clear cell renal cell carcinoma, *SD* standard deviation, *BMI* body mass index, *RN* radical nephrectomy, *PN* partial nephrectomy
 **P* < 0.05

in the corticomedullary phase and subsequently relative hypoenhancement in the delayed phase. Positive is defined as the threshold ratio greater than or equal to 1.5, while negative otherwise. Disagreements were resolved by consensus. Figure 2 shows the ccLS algorithm and image interpretation. Figure 3 shows the imaging parameters of clear cell likelihood score (ccLS).

In the final analysis, the evaluation result was utilized to compare the differences in the ccLS score between EAML

and ccRCC and evaluate the diagnostic performance of ccLS for the two diseases. EAML is often more difficult to distinguish from ccRCC at smaller sizes. Considering the differences in preoperative diagnosis difficulty, treatment plan, and prognosis for small renal masses (SRM; ≤ 4 cm) and large renal masses (LRM; > 4 cm), then all cases were reclassified into two subgroups with a maximum diameter of 4 cm as the dividing line, and the effect of tumor size on the ccLS score was evaluated.

Fig. 4 A Sankey diagram illustrating the scmap cluster projection of the diagnosis of the cases, gender and age composition, tumor location, symptom, smoking history, drinking history, hypertension history and diabetes history as well as surgery

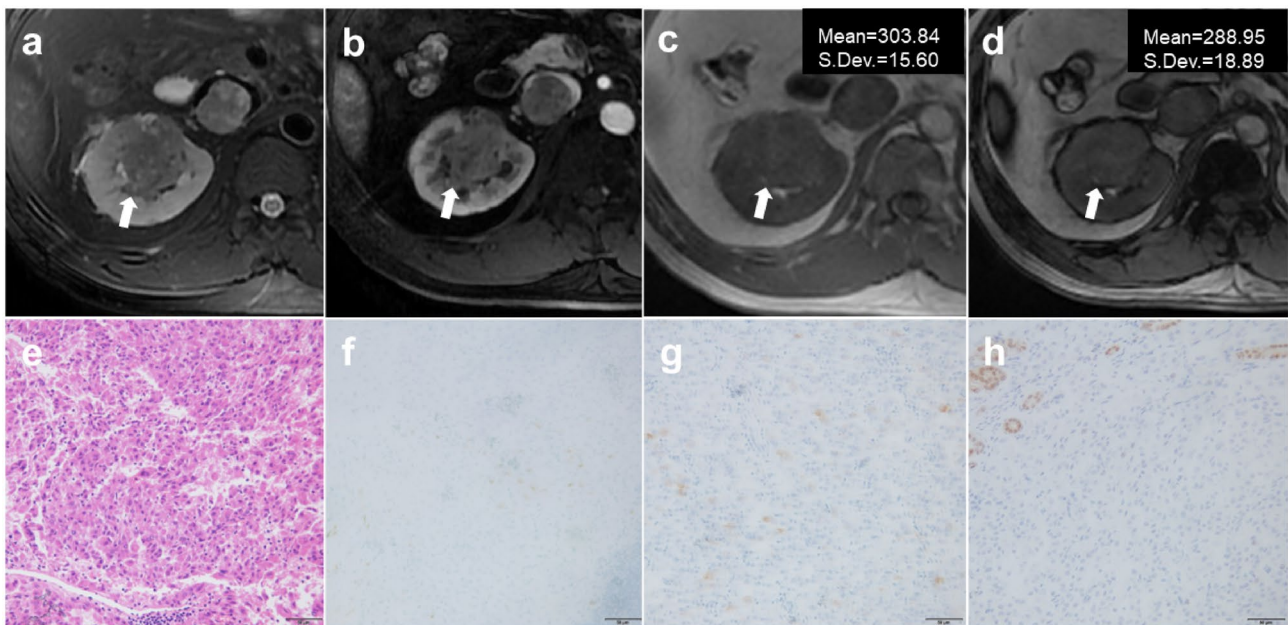
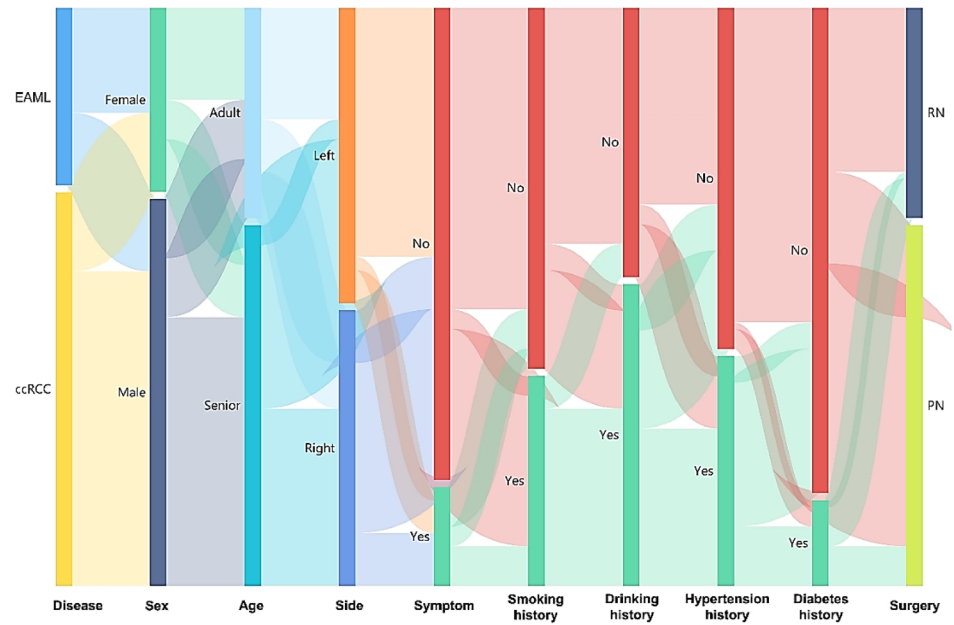


Fig. 5 Images in a 28-year-old man with a right-sided epithelioid angiomyolipoma mass (**a–h**). The lesion shows heterogeneous hypointense (arrowhead) on axial T2-weighted MRI scan (**a**), heterogeneous mild enhancement that is lower to the adjacent renal cortex (arrowhead) on axial corticomedullary-phase contrast-enhanced

T1-weighted image (**b**). Axial T1-weighted gradient-echo in-phase (**c**) and opposed-phase (**d**) images indicate the absence of microscopic fat in the mass (arrowhead), and photomicrograph helps confirm the diagnosis of EAML (**e–h**). The lesion was classified as cCLS 1 according to clear cell likelihood score

Pathologic analysis

All pathologic results of tumors have been reviewed retrospectively by an experienced uropathologist (X.H.D., with

20 years of experience) following the 2016 World Health Organization Classification of Tumors of the Urinary System and Male Genital Organs [9].

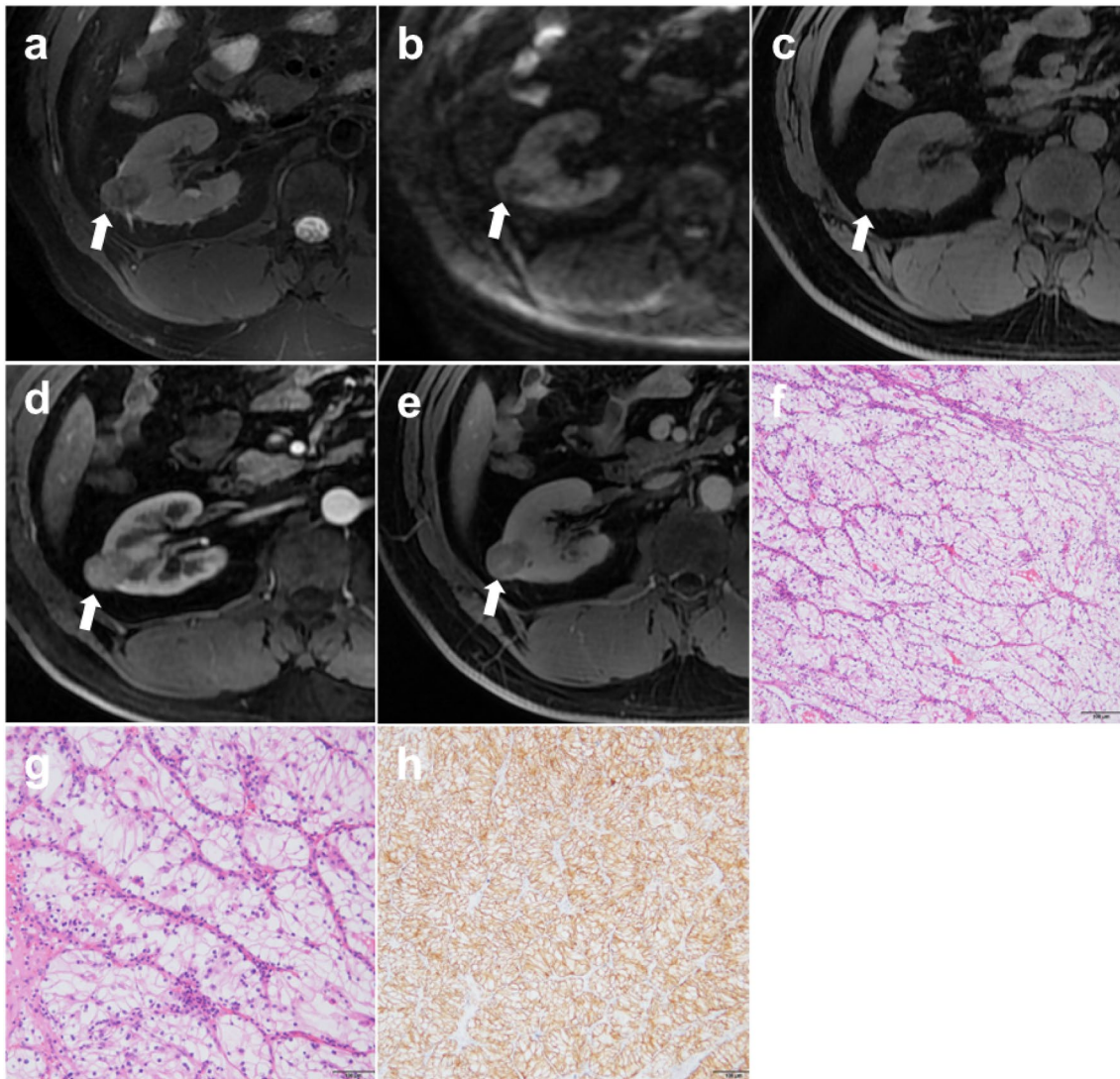


Fig. 6 Images in a 47-year-old man with a right-sided clear cell renal cell carcinoma mass (**a–h**). The lesion shows hypointense (arrowhead) on axial T2-weighted MRI scan (**a**), no marked restriction on DWI (**b**), intense heterogeneous enhancement that is higher to the adjacent renal cortex (arrowhead) on axial corticomedullary-phase

contrast-enhanced T1-weighted image. Quantitative analysis demonstrated ADER < 1.5 (**c–e**), and photomicrograph helps confirm the diagnosis of ccRCC (**f–h**). The lesion was classified as ccLS 4 according to clear cell likelihood score

Statistical analysis

All data were analyzed statistically using Medcalc 19.5.1 and Stata/MP16.0. Quantitative data were presented as mean \pm standard deviation ($\bar{x} \pm SD$). Independent sample t-test was used to compare the continuous variables of normal distribution. Mann Whitney U test was used to compare rank data and non-normally distributed variables. Cohen's kappa coefficient was used to evaluate interobserver agreement, with kappa values of < 0.20 being considered poor, 0.2–0.40 as fair, 0.41–0.60 as moderate,

0.61–0.80 as good, 0.80–1.00 as excellent. The difference of the ccLS score between EAML and ccRCC in the whole study cohort and in two subgroups was compared using analysis of variance. And the receiver operating characteristic curve (ROC) analysis was performed to evaluate the performance of the ccLS score for distinguishing the two diseases. $P < 0.05$ indicated a statistically significant.

Table 2 Imaging features and score distribution of EAML and ccRCC

	EAML					All (%)	ccRCC					All (%)
	1	2	3	4	5		1	2	3	4	5	
T2 signal intensity												
Hyperintense	0	0	0	0	1	1 (3)	0	0	0	0	27	27 (45)
Isointense	0	3	1	2	0	6 (20)	0	1	6	12	0	19 (32)
Hypointense	18	1	3	1	0	23 (77)	0	2	5	7	0	14 (23)
Enhancement												
Intense	0	1	3	3	1	8 (27)	0	2	10	19	27	58 (96)
Moderate	0	3	1	0	0	4 (13)	0	0	1	0	0	1 (2)
Mild	18	0	0	0	0	18 (60)	0	1	0	0	0	1 (2)
Microscopic fat												
ADER < 1.5	10	2	2	3	0	17 (57)	0	1	9	16	24	50 (83)
Cystic change	6	2	0	2	1	11 (37)	0	1	2	6	26	35 (58)
Restricted on DWI	16	4	3	3	1	27 (90)	0	3	8	9	10	30 (50)

EAML renal epithelioid angiomyolipoma, ccRCC clear cell renal cell carcinoma, ADER $SI_{art} - SI_{pre} / SI_{del} - SI_{pre}$, DWI diffusion-weighted images

Table 3 The scores of EAML and ccRCC

Group	ccLS1-2	ccLS3	ccLS4-5	All
EAML	22 (74%)	4 (13%)	4 (13%)	30 (100%)
ccRCC	3 (5%)	11 (18%)	46 (77%)	60 (100%)

$\chi^2 = 48.360, v = 2, P < 0.001$

ccLS clear cell likelihood score, EAML renal epithelioid angiomyolipoma, ccRCC clear cell renal cell carcinoma

Table 4 Comparison the scores of EAML and ccRCC in the whole study cohort and two subgroups

Group	ccLS1-2	ccLS3	ccLS4-5	All
SRM	13 (23%)	12 (21%)	32 (56%)	57 (63%)
LRM	12 (36%)	3 (9%)	18 (56%)	33 (37%)
All	25 (28%)	15 (17%)	50 (55%)	90 (100%)

F = 0.249, v = 2, P = 0.780 > 0.05

ccLS clear cell likelihood score, EAML renal epithelioid angiomyolipoma, ccRCC clear cell renal cell carcinoma, SRM small renal masses, LRM large renal masses

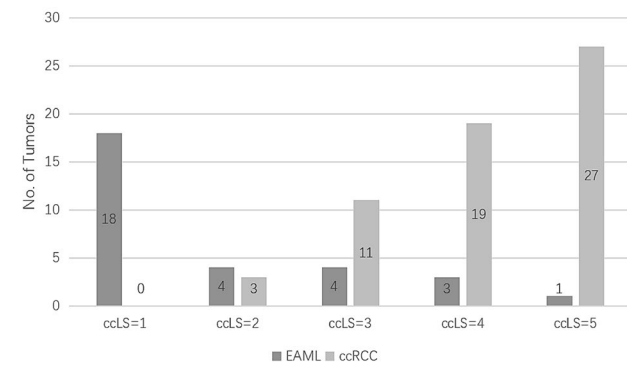


Fig. 7 Histology distribution of cohort by clear cell likelihood score (ccLS). ccRCC clear cell renal cell carcinoma; EAML renal epithelioid angiomyolipoma

Results

Patient characteristics

A total of 90 lesions in 87 patients were included in this study and were divided into the EAML group (n = 27, one patient had four masses) and the ccRCC group (n = 60).

There were 56 males (EAML, n=11; ccRCC, n=45) and 31 females (EAML, n=16; ccRCC, n=15), aged 27 to 78 years (mean age 55 ± 11 years). Patient demographics and clinical characteristics are shown in Table 1 and Fig. 4. There were statistically significant differences in age, gender, smoking history, drinking history, hypertension history, and diabetes history between the two groups.

Imaging features and the cLS score

The Cohen’s kappa coefficient of two radiologists for the ccLS system to differentiate EAML from ccRCC was 0.71 (Table E5), indicating good consistency between the two radiologists.

In the EAML group (Fig. 5), 23 (76.7%) lesions showed hypointense on T₂WI, 18 (60.0%) lesions showed mild enhancement on the corticomedullary phase, 14 (46.7%) lesions showed microscopic fat, 27 (90.0%) lesions showed restriction on DWI, and cystic degeneration occurred in 11 (36.7%) lesions, and arterial-delayed enhancement ratio (ADER) < 1.5 in 17 (56.7%) lesions. In the ccRCC group (Fig. 6), 27 (45.0%) lesions showed hyperintense on T₂WI,

Fig. 8 Receiver operating characteristic curve (ROC) shows the diagnostic performance of clear cell likelihood score (ccLS) in the whole study cohort, the small renal masses (SRM) subgroup, and the large renal masses (LRM) subgroup. In the whole study cohort, area under the curve (AUC) was 0.913. In the SRM subgroup, AUC was 0.969. In the LRM subgroup, AUC was 0.842. The Youden index is maximized at a cutoff value of 2

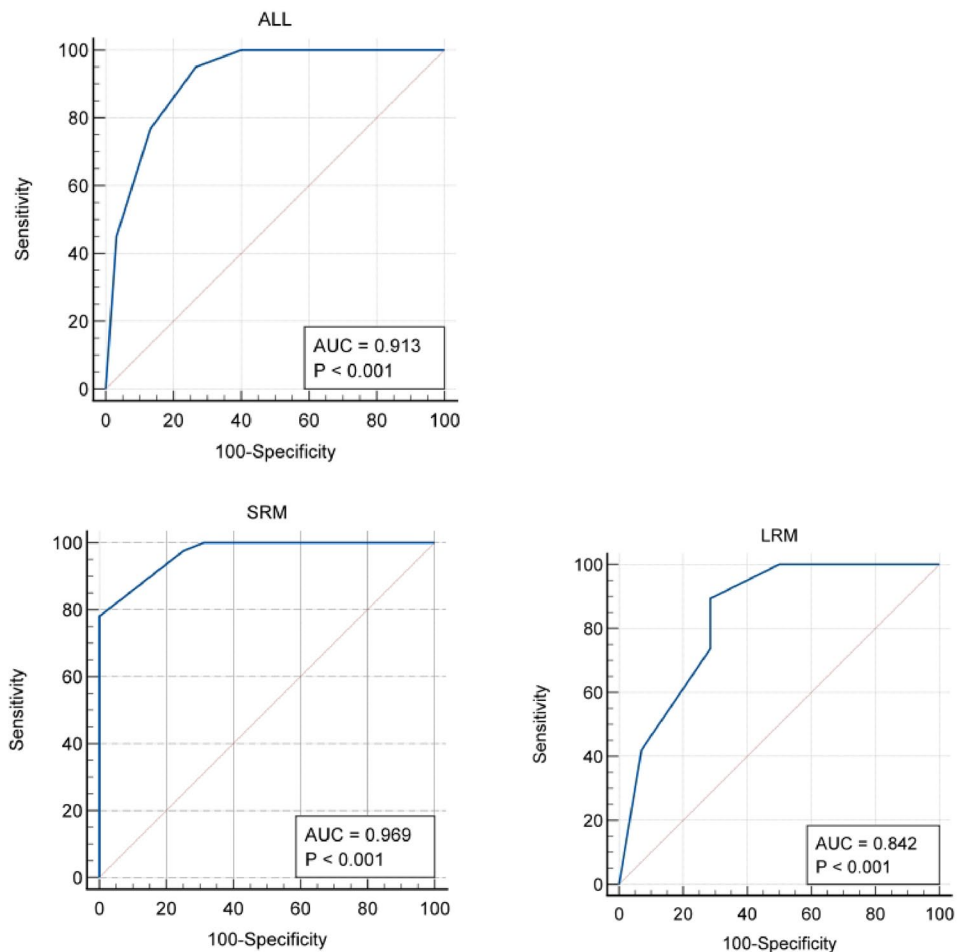


Table 5 Diagnostic performance of clear cell likelihood score (ccLS)

	SRM	LRM	All
Number of lesions	57 (63%)	33 (37%)	90 (100%)
Accuracy	91.2% (80.7%–97.1%)	81.8% (64.5%–93.0%)	87.8% (79.2%–93.7%)
Sensitivity	75.0% (47.6%–92.7%)	89.5% (66.9%–98.7%)	95.0% (86.1%–99.0%)
Specificity	97.6% (87.1%–99.9%)	71.4% (41.9%–91.6%)	73.3% (54.1%–87.7%)
PPV	90.9% (81.0%–95.9%)	81.0% (64.7%–90.8%)	87.7% (79.7%–92.8%)
NPV	92.3% (62.9%–98.8%)	83.3% (56.4%–95.1%)	88.0% (70.4%–95.8%)
The Youden index	0.780	0.609	0.683

95% credible interval shown in parentheses

SRM small renal masses, LRM large renal masses, PPV positive predictive value, NPV negative predictive value

58 (96.7%) lesions showed intense enhancement on the corticomedullary phase, 39 (65.0%) lesions showed microscopic fat, 30 (50.0%) lesions showed restriction on DWI, and cystic degeneration occurred in 35 (58.3%) lesions, and ADER < 1.5 in 50 (83.3%) lesions. There were significant differences in T2 signal intensity, corticomedullary enhancement, microscopic fat, cystic degeneration, and restricted diffusion on DWI between the two groups (*P*

< 0.05). Table 2 shows the imaging features and the ccLS score of the EAML and ccRCC groups. Table 3 and Fig. 7 show the distribution of the ccLS score between EAML and ccRCC groups, the difference was statistically significant (*P* < 0.001).

All lesions were divided into the SRM subgroup and the LRM subgroup. The distribution of the ccLS score for the two subgroups is shown in Table 4. The diagnostic

performance of the whole study cohort and the two subgroups with the ccLS score was comparable ($P = 0.780$), indicating that the ccLS scores of the two diseases were unaffected by tumor size.

Diagnostic performance of ccLS

ROC curves are shown in Fig. 8, with AUC of all EAML and ccRCC in the whole study cohort was 0.913 [95% confidence interval CI 0.834, 0.962], with statistical significance ($P < 0.001$). The point with the maximum Youden index was chosen as the cut-off value, that is, defining EAML as scores ≤ 2 and defining ccRCC as scores > 2 . The overall accuracy, sensitivity, specificity, positive predictive value (PPV), and negative predictive value (NPV) were 87.8%, 95.0%, 73.3%, 87.7%, and 88.0%. The diagnostic performance of ccLS for EAML and ccRCC is shown in Table 5. In the SRM subgroup, AUC was 0.969 (95% CI 0.885–0.967), with statistical significance ($P < 0.001$), and a cut-off value of ≤ 2 was able to distinguish EAML from ccRCC with an accuracy, sensitivity, specificity, PPV and NPV of 91.2%, 75.0%, 97.6%, 90.9% and 92.3%, respectively. In the LRM subgroup, AUC was 0.842 (95% CI 0.673–0.945), with statistical significance ($P < 0.001$), and a cut-off value of ≤ 2 was able to distinguish two entities with accuracy, sensitivity, specificity, PPV and NPV of 81.8%, 89.5%, 71.4%, 81.0%, and 83.3%, respectively.

Discussion

In this study, we evaluated ccLS to differentiate EAML and ccRCC, and found the best cutoff value to distinguish the two diseases through the ROC curve. The Youden index is maximized at a cutoff value of 2, that is, a ccLS score of 1–2 points is diagnosed as EAML, while a ccLS score of 3–5 points is diagnosed as ccRCC. Our study indicated that ccLS as a standardized grading system demonstrates high performance in the differentiating EAML from ccRCC.

In line with the previous study [34], we found that high NPV for ccLS ≤ 2 and high PPV for ccLS ≥ 4 are helpful for differential diagnosis (AUC 0.913, $P < 0.001$). EAML contains a large number of epithelioid cells [7] which may result in hypointensity on T2-Weighted imaging, and mild enhancement on the corticomedullary phase. This explains why most EAMLs have a ccLS score of 1–2. The pathology of ccRCC is characterized by clear cytoplasm, and clear cell membrane, distributed in the hyper-vascularized stroma [35]. The tumor is usually isointense—hyperintense on T2-Weighted imaging, and intensely enhances on the corticomedullary phase. This is why the ccLS score of 4–5 in most ccRCC is different on the 1–2 score of EAML. In

addition, there was a good interobserver agreement between the two abdominal radiologists ($k = 0.71$). Previous studies showed moderate consistency ($k = 0.53$) in the assessment of renal tumors with the ccLS score [34, 36]. And as reported by Dunn [30], the interreader agreement for fpAML in cT1a (0.24–0.33) and cT1b (– 0.14 to 0.21) masses ranged from poor to fair. One explanation could be that only two pathological subtypes were included in our study, reducing the possibility of confusion.

The proportion of EAML with the ccLS score 3–5 is approximately 26.7% (8/30). The reason could be that EAML has low-grade malignant potential, few of them showing invasive growth and similar MR imaging features to ccRCC, such as cystic change, hemorrhage, necrosis, and microscopic fat. It has been reported that EAML could invade the renal sinus, perirenal fat, renal vein, the infrarenal vena cava, and local lymph nodes, as well as distant metastasis to the lung, liver, and mesentery [10, 37]. Three instances of ccRCC were misdiagnosed as EAML due to the ccLS score of 2. Twelve percent of ccLS ≤ 2 tumors were evaluated to be ccRCC in our study which is similar to the 10% reported by Ibrahim et al and the 11% reported by Steinberg et al [36, 38]. These lesions were iso-hypo signal intensities on T2WI, ADER > 1.5 , and had restriction at DWI. Therefore, these lesions have a ccLS score of 2.

Small tumors are more difficult to distinguish from MR images [33]. Nevertheless, In accordance with Dunn et al [30], the AUC of ccLS in the SRM group was as high as 0.97 in our study, suggesting that ccLS would be useful as a diagnostic tool for cT1a stage EAML and ccRCC. Steinberg [36] concluded that the ccLS score was not only suitable for small renal masses but also had a great diagnostic performance for renal masses of all sizes and stages. Our present study shows that the diagnostic accuracy of the ccLS score for the SRM subgroup is 91.2%, and for the LRM subgroup is 81.8%, respectively. This indicates that the lesional size increased and led to an increased rate of misdiagnosis. However, the diagnostic performance of the scoring system for both diseases remained unaffected by the size of the renal tumor ($P = 0.780$). Tumor size may be a potential factor affecting the ccLS threshold for the whole study cohort and the LRM group. In accordance with the previous study [39], when the tumor size is larger, it is more likely to be malignant and more likely to metastasize.

ccLS provides junior radiologists and non-abdominal radiologists with a novel approach to diagnosing renal tumors [40, 41], even when senior abdominal radiologists have difficulty distinguishing rare subtypes from common subtypes. But this approach should take into account patient factors (eg, age, gender, clinical presentation) and would need further validation before being accepted on a clinical basis [42]. Similar to previous studies [1, 2, 42–44], the age,

gender, smoking, drinking, hypertension, and diabetes in the two groups were also important for differentiation.

This study has some limitations. First, this study was a retrospective study with only 27 cases (30 lesions) of EAML, but there is the largest cohort related to EAML at present. Second, EAML may also be mistaken for other renal tumors, including poor fat AML and non-clear cell RCC. Further research will be conducted to evaluate the value of ccLS in the diagnosis and differential diagnosis of other renal tumors. Finally, the imaging assessment in this study was based on fat-saturated T2-weighted single-shot fast spin-echo images, which may therefore impact the image contrast [29].

In conclusion, ccLS could be an alternative approach in the differential diagnosis between EAML and ccRCC, thus potentially helping the management of EAML and ccRCC.

Supplementary Information The online version contains supplementary material available at <https://doi.org/10.1007/s00261-023-04034-5>.

Acknowledgements We acknowledge the financial support from the National Natural Science Foundation of China (Grant 81971580 and 82271951 and 81771785) and Beijing Municipal Natural Science Foundation (Grant 7222167).

Declarations

Conflict of interest The author declares that there are no disclosures relevant to the subject of this article.

References


- He W, Chevillet JC, Sadow PM et al (2013) Epithelioid angiomyolipoma of the kidney: pathological features and clinical outcome in a series of consecutively resected tumors. *Mod Pathol* 26(10):1355–64. <https://doi.org/10.1038/modpathol.2013.72>
- Bao HL, Chen X, An YX et al (2017) Clinical and pathologic analysis of 414 cases of renal angiomyolipoma in a single institution. *Chin J Pathol* 46(6):378–82. <https://doi.org/10.3760/cma.j.issn.0529-5807.2017.06.003>
- Katabathina VS, Vikram R, Nagar AM et al (2010) Mesenchymal neoplasms of the kidney in adults: imaging spectrum with radiologic-pathologic correlation. *Radiographics* 30(6):1525–40. <https://doi.org/10.1148/rg.306105517>
- Montironi, R, Cheng, L, Scarpelli, M et al (2016) Pathology and Genetics: Tumours of the Urinary System and Male Genital System: Clinical Implications of the 4th Edition of the WHO Classification and Beyond. *European urology*, 70(1), 120–123. <https://doi.org/10.1016/j.eururo.2016.03.011>
- Park HK, Zhang S, Wong MKK et al (2007) Clinical presentation of epithelioid angiomyolipoma. *Int J Urol* 14(1):21–5. <https://doi.org/10.1111/j.1442-2042.2006.01665.x>
- Warakaulle DR, Phillips RR, Turner GDH et al (2004) Malignant monotypic epithelioid angiomyolipoma of the kidney. *Clin Radiol* 59(9):849–52. <https://doi.org/10.1016/j.crad.2004.02.009>
- Tsukada J, Jinzaki M, Yao M et al (2013) Epithelioid angiomyolipoma of the kidney: radiological imaging. *Int J Urol* 20(11):1105–11. <https://doi.org/10.1111/iju.12117>
- Eble JN, Amin MB, Young RH (1997) Epithelioid angiomyolipoma of the kidney: a report of five cases with a prominent and diagnostically confusing epithelioid smooth muscle component. *Am J Surg Pathol* 21(10):1123–30. <https://doi.org/10.1097/0000478-199710000-00001>
- Moch H, Cubilla AL, Berney, DM et al (2022) The 2022 World Health Organization Classification of Tumours of the Urinary System and Male Genital Organs-Part A: Renal, Penile, and Testicular Tumours. *European urology*, 82(5), 458–468. <https://doi.org/10.1016/j.eururo.2022.06.016>
- Froemming AT, Boland J, Chevillet J et al (2013) Renal epithelioid angiomyolipoma: imaging characteristics in nine cases with radiologic-pathologic correlation and review of the literature. *AJR Am J Roentgenol* 200(2):W178–86. <https://doi.org/10.2214/AJR.12.8776>
- Guo R, Kang SH, Zhong Y et al (2018) Magnetic resonance imaging findings and differential diagnosis of renal epithelioid angiomyolipoma comparing with renal non-epithelioid angiomyolipoma. *Zhonghua Yi Xue Za Zhi* 98(45):3701–3704. <https://doi.org/10.3760/cma.j.issn.0376-2491.2018.45.014>
- Muglia VF, Prando A (2015) Renal cell carcinoma: histological classification and correlation with imaging findings. *Radiol Bras* 48(3):166–74. <https://doi.org/10.1590/0100-3984.2013.1927>
- Gnarra JR, Tory K, Weng Y et al (1994) Mutations of the VHL tumour suppressor gene in renal carcinoma. *Nat Genet* 7(1):85–90. <https://doi.org/10.1038/ng0594-85>
- Sonpavde G, Willey CD, Sudarshan S (2014) Fibroblast growth factor receptors as therapeutic targets in clear-cell renal cell carcinoma. *Expert Opin Investig Drugs* 23(3):305–15. <https://doi.org/10.1517/13543784.2014.871259>
- Chevillet JC, Lohse CM, Zincke H et al (2004) Sarcomatoid renal cell carcinoma an examination of underlying histologic subtype and an analysis of associations with patient outcome. *Am J Surg Pathol* 28(4):435–41. <https://doi.org/10.1097/0000478-200404000-00002>
- Marconi L, Dabestani S, Lam TB et al (2016) Systematic review and meta-analysis of diagnostic accuracy of percutaneous renal tumour biopsy. *Eur Urol* 69(4):660–73. <https://doi.org/10.1016/j.eururo.2015.07.072>
- Lim CS, Schieda N, Silverman SG (2019) Update on indications for percutaneous renal mass biopsy in the era of advanced CT and MRI. *AJR Am J Roentgenol* 27:1–10. <https://doi.org/10.2214/AJR.19.21093>
- Kim TM, Ahn H, Lee HJ et al (2022) Differentiating renal epithelioid angiomyolipoma from clear cell carcinoma: using a radiomics model combined with CT imaging characteristics. *Abdom Radiol (NY)*. 47(8):2867–2880. <https://doi.org/10.1007/s00261-022-03571-9>
- Hötter AM, Mazaheri Y, Wibmer A et al (2017) Differentiation of clear cell renal cell carcinoma from other renal cortical tumors by use of a quantitative multiparametric MRI approach. *AJR Am J Roentgenol* 208(3):W85–W91. <https://doi.org/10.2214/AJR.16.16652>
- Cornelis F, Tricaud E, Lasserre AS et al (2014) Routinely performed multiparametric magnetic resonance imaging helps to differentiate common subtypes of renal tumours. *Eur Radiol* 24(5):1068–80. <https://doi.org/10.1007/s00330-014-3107-z>
- Allen BC, Tirman P, Jennings Clingan M et al (2014) Characterizing solid renal neoplasms with MRI in adults. *Abdom Imaging* 39(2):358–87. <https://doi.org/10.1007/s00261-014-0074-4>
- Cong X, Zhang J, Xu X et al (2018) Renal epithelioid angiomyolipoma: magnetic resonance imaging characteristics.

- Abdom Radiol (NY) 43(10):2756–63. <https://doi.org/10.1007/s00261-018-1548-6>
23. Zhong Y, Shen Y, Pan J et al (2017) Renal epithelioid angiomyolipoma: MRI findings. *Radiol Med* 122(11):814–21. <https://doi.org/10.1007/s11547-017-0788-9>
 24. Wang D, Gong G, Fu Y et al (2022) CT imaging findings of renal epithelioid lipid-poor angiomyolipoma. *Eur Radiol* 32(7):4919–4930. <https://doi.org/10.1007/s00330-021-08528-y>
 25. Cui L, Zhang JG, Hu XY et al (2012) CT imaging and histopathological features of renal epithelioid angiomyolipomas. *Clin Radiol* 67(12):e77–82. <https://doi.org/10.1016/j.crad.2012.08.006>
 26. Roussel E, Capitanio U, Kutikov A et al (2022) Novel imaging methods for renal mass characterization: a collaborative review. *Eur Urol* 81(5):476–88. <https://doi.org/10.1016/j.eururo.2022.01.040>
 27. Kay FU, Pedrosa I (2017) Imaging of solid renal masses. *Radiol Clin North Am* 55(2):243–58. <https://doi.org/10.1016/j.rcl.2016.10.003>
 28. Canvasser NE, Kay FU, Xi Y et al (2017) Diagnostic accuracy of multiparametric magnetic resonance imaging to identify clear cell renal cell carcinoma in cT1a renal masses. *J Urol* 198(4):780–6. <https://doi.org/10.1016/j.juro.2017.04.089>
 29. Pedrosa I, Cadeddu JA (2022) How we do it: managing the indeterminate renal mass with the MRI clear cell likelihood score. *Radiology* 302(2):256–69. <https://doi.org/10.1148/radiol.210034>
 30. Dunn M, Linehan V, Clarke SE et al (2022) Diagnostic performance and interreader agreement of the MRI clear cell likelihood score for characterization of cT1a and cT1b solid renal masses: an external validation study. *AJR Am J Roentgenol* 219(5):793–803. <https://doi.org/10.2214/AJR.22.27378>
 31. Kay FU, Pedrosa I (2018) Imaging of solid renal masses. *Urol Clin North Am*. 2018;45(3):311–330. <https://doi.org/10.1016/j.ucl.2018.03.013>
 32. Sun MRM, Ngo L, Genega EM et al (2009) Renal cell carcinoma: dynamic contrast-enhanced MR imaging for differentiation of tumor subtypes--correlation with pathologic findings. *Radiology* 250(3):793–802. <https://doi.org/10.1148/radiol.2503080995>
 33. Sasiwimonphan K, Takahashi N, Leibovich BC et al (2012) Small (<4 cm) renal mass: differentiation of angiomyolipoma without visible fat from renal cell carcinoma utilizing MR imaging. *Radiology* 263(1):160–8. <https://doi.org/10.1148/radiol.12111205>
 34. Johnson BA, Kim S, Steinberg RL et al (2019) Diagnostic performance of prospectively assigned clear cell Likelihood scores (ccLS) in small renal masses at multiparametric magnetic resonance imaging. *Urol Oncol* 37(12):941–6. <https://doi.org/10.1016/j.urolonc.2019.07.023>
 35. Kuroda N, Karashima T, Inoue K et al (2015) Review of renal cell carcinoma with rhabdoid features with focus on clinical and pathobiological aspects. *Pol J Pathol* 66(1):3–8. <https://doi.org/10.5114/pjp.2015.51147>
 36. Steinberg RL, Rasmussen RG, Johnson BA et al (2021) Prospective performance of clear cell likelihood scores (ccLS) in renal masses evaluated with multiparametric magnetic resonance imaging. *Eur Radiol* 31(1):314–24. <https://doi.org/10.1007/s00330-020-07093-0>
 37. Brimo F, Robinson B, Guo C et al (2010) Renal epithelioid angiomyolipoma with atypia: a series of 40 cases with emphasis on clinicopathologic prognostic indicators of malignancy. *Am J Surg Pathol* 34(5):715–22. <https://doi.org/10.1097/PAS.0b013e3181d90370>
 38. Ibrahim, A., Pelsser, V., Anidjar, M et al (2023). Performance of clear cell likelihood scores in characterizing solid renal masses at multiparametric MRI: an external validation study. *Abdominal radiology*, 48(3), 1033–1043. <https://doi.org/10.1007/s00261-023-03799-z>
 39. Lee H, Lee JK, Kim K et al (2016) Risk of metastasis for T1a renal cell carcinoma. *World J Urol* 34(4):553–9. <https://doi.org/10.1007/s00345-015-1659-4>
 40. Tse J R (2022) Editorial Comment: Clear Cell Likelihood Score--Another Step Toward Noninvasive Risk Stratification. *AJR. American journal of roentgenology*, 17:11. <https://doi.org/10.2214/AJR.22.28087>
 41. Mileto A, Potretzke T A (2022) Standardized Evaluation of Small Renal Masses Using the MRI Clear Cell Likelihood Score. *Radiology*, 303(3):600–602. <https://doi.org/10.1148/radiol.220054>
 42. Rasmussen RG, Xi Y, Sibley RC et al (2022) Association of clear cell likelihood score on MRI and growth kinetics of small solid renal masses on active surveillance. *AJR Am J Roentgenol* 218(1):101–10. <https://doi.org/10.2214/AJR.21.25979>
 43. Kay FU, Canvasser NE, Xi Y et al (2018) Diagnostic performance and interreader agreement of a standardized MR imaging approach in the prediction of small renal mass histology. *Radiology* 287(2):543–53. <https://doi.org/10.1148/radiol.2018171557>
 44. Li XQ, Chang T (2017) The application value of support vector machine in CT differential diagnosis of renal epithelioid angiomyolipoma and clear cell renal cell carcinoma. *Chinese Journal of CT and MRI* 2017; 10(10):91–3. <https://doi.org/10.3969/j.issn.1672-5131.2017.10.029>

Publisher's Note Springer Nature remains neutral with regard to jurisdictional claims in published maps and institutional affiliations.

Springer Nature or its licensor (e.g. a society or other partner) holds exclusive rights to this article under a publishing agreement with the author(s) or other rightsholder(s); author self-archiving of the accepted manuscript version of this article is solely governed by the terms of such publishing agreement and applicable law.

Authors and Affiliations

Yu-Wei Hao¹ · Yun Zhang^{1,2} · Hui-Ping Guo¹ · Wei Xu¹ · Xu Bai¹ · Jian Zhao¹ · Xiao-Hui Ding³ · Sheng Gao⁴ · Meng-Qiu Cui¹ · Bai-Chuan Liu¹ · Hui-Yi Ye¹ · Hai-Yi Wang¹ 

✉ Hai-Yi Wang
wanghaiyi301@outlook.com

Yu-Wei Hao
haoweiveiwei@outlook.com

Yun Zhang
zhangyunhappy12345@163.com

Hui-Ping Guo
guohuiping1015@126.com

Wei Xu
xwwish@163.com

Xu Bai
baixu361@126.com

Jian Zhao
zhaojian419115679@163.com

Xiao-Hui Ding
aprilisding@163.com

Sheng Gao
284473644@qq.com

Meng-Qiu Cui
acuimengqiu@163.com

Bai-Chuan Liu
medlbc0413@126.com

Hui-Yi Ye
13701100368@163.com

- ¹ Department of Radiology, First Medical Center, Chinese PLA General Hospital, No. 28 Fuxing Road, Haidian District, Beijing 100853, China
- ² Department of Radiology, Sixth Medical Center, Chinese PLA General Hospital, Beijing, China
- ³ Department of Pathology, First Medical Center, Chinese PLA General Hospital, Beijing, China
- ⁴ Department of Radiology, Linyi Central Hospital, Shandong, China